



## Two Functional Channels from Primary Visual Cortex to Dorsal Visual Cortical Areas

N. Harumi Yabuta, *et al.*  
*Science* **292**, 297 (2001);  
DOI: 10.1126/science.1057916

**The following resources related to this article are available online at [www.sciencemag.org](http://www.sciencemag.org) (this information is current as of January 6, 2007):**

**Updated information and services**, including high-resolution figures, can be found in the online version of this article at:

<http://www.sciencemag.org/cgi/content/full/292/5515/297>

A list of selected additional articles on the Science Web sites **related to this article** can be found at:

<http://www.sciencemag.org/cgi/content/full/292/5515/297#related-content>

This article **cites 28 articles**, 11 of which can be accessed for free:

<http://www.sciencemag.org/cgi/content/full/292/5515/297#otherarticles>

This article has been **cited by** 36 article(s) on the ISI Web of Science.

This article has been **cited by** 11 articles hosted by HighWire Press; see:

<http://www.sciencemag.org/cgi/content/full/292/5515/297#otherarticles>

This article appears in the following **subject collections**:

Neuroscience

<http://www.sciencemag.org/cgi/collection/neuroscience>

Information about obtaining **reprints** of this article or about obtaining **permission to reproduce this article** in whole or in part can be found at:

<http://www.sciencemag.org/help/about/permissions.dtl>

19. A. El Manira, W. Zhang, E. Svensson, N. Bussières, *J. Neurosci.* **17**, 1786 (1997).  
 20. G. G. Holz, R. M. Kream, A. Spiegel, K. Dunlap, *J. Neurosci.* **9**, 657 (1989).  
 21. A. C. Dolphin et al., *Biochem. Soc. Trans.* **21**, 391 (1993).  
 22. S. Herlitze et al., *Nature* **380**, 258 (1996).  
 23. S. R. Ikeda, *Nature* **380**, 255 (1996).  
 24. M. De Waard et al., *Nature* **385**, 446 (1997).  
 25. N. Qin, D. Platano, R. Olcese, E. Stefani, L. Birnbaumer, *Proc. Natl. Acad. Sci. U.S.A.* **94**, 8866 (1997).  
 26. GST fusion proteins encoded by pGEX vectors were produced in *Escherichia coli* by standard methods. Standard conditions for binding studies employed 200- $\mu$ l reactions containing 0.02 M Hepes (pH 7.2), 0.15 M KCl, 0.5% Triton X-100, 0.03% CHAPS, and 1% cold fish skin gelatin. Ternary SNARE complexes were formed by overnight incubation at 4°C of SNAP-25B, syntaxin1A, or VAMP11, each at 1  $\mu$ M. Incubations were for 1 hour at 4°C, after which beads were recovered by centrifugation and washed three

times in 500  $\mu$ l of assay buffer before solubilization in sample buffer for SDS-polyacrylamide gel electrophoresis. Electrophoresed samples were transferred to nitrocellulose for immunoblotting with a polyclonal rabbit antibody generated against G $\beta$  used at a dilution of 1:500. Enhanced chemiluminescence was used for detection. Horseradish peroxidase-conjugated goat anti-rabbit secondary antibodies were used at a dilution of 1:20,000.  
 27. S. E. Jarvis, J. M. Magga, A. M. Beedle, J. E. Braun, G. W. Zamponi, *J. Biol. Chem.* **275**, 6388 (2000).  
 28. E. Reuveny et al., *Nature* **370**, 143 (1994).  
 29. C. L. Huang, P. A. Slesinger, P. J. Casey, Y. N. Jan, L. Y. Jan, *Neuron* **15**, 1133 (1995).  
 30. P. Kofuji, N. Davidson, H. A. Lester, *Proc. Natl. Acad. Sci. U.S.A.* **92**, 6542 (1995).  
 31. D. E. Logothetis, Y. Kurachi, J. Galper, E. J. Neer, D. E. Clapham, *Nature* **325**, 321 (1987).  
 32. T. Takahashi, I. D. Forsythe, T. Tsujimoto, M. Barnes-Davies, K. Onodera, *Science* **274**, 594 (1996).  
 33. R. R. Mirotnik, X. Zheng, E. F. Stanley, *J. Neurosci.* **20**, 7614 (2000).

34. E. M. Silinsky, *J. Physiol. (London)* **346**, 243 (1984).  
 35. \_\_\_\_\_, C. S. Solsona, *J. Physiol. (London)* **457**, 315 (1992).  
 36. M. Umemiya, A. J. Berger, *J. Neurophysiol.* **73**, 1192 (1995).  
 37. J. H. Singer, A. J. Berger, *Sleep* **19**, S146 (1996).  
 38. A. Luini, M. A. De Matteis, *J. Neurochem.* **54**, 30 (1990).  
 39. We are grateful to A. Bohm, Y. Daaka, and B. M. Willardson for their generous gifts of ct-GRK2, pGex ct-GRK5, and GST-Phosducin, respectively. We thank N. Skiba for helpful suggestions regarding preparation of ct-GRK2 and G $\beta$  $\gamma$  for microinjection and E. Silinsky and E. Mugnaini for their critical reading of the manuscript. This work was funded by grants from the National Eye Institute (H.E.H.), the National Institute of Diabetes and Digestive and Kidney Diseases (T.F.J.M.), and the National Institute of Neurological Disorders and Stroke (S.A.).

5 January 2001; accepted 15 March 2001

## Two Functional Channels from Primary Visual Cortex to Dorsal Visual Cortical Areas

N. Harumi Yabuta, Atomu Sawatari,\* Edward M. Callaway†

Relationships between the M and P retino-geniculo-cortical visual pathways and "dorsal" visual areas were investigated by measuring the sources of local excitatory input to individual neurons in layer 4B of primary visual cortex. We found that contributions of the M and P pathways to layer 4B neurons are dependent on cell type. Spiny stellate neurons receive strong M input through layer 4C $\alpha$  and no significant P input through layer 4C $\beta$ . In contrast, pyramidal neurons in layer 4B receive strong input from both layers 4C $\alpha$  and 4C $\beta$ . These observations, along with evidence that direct input from layer 4B to area MT arises predominantly from spiny stellates, suggest that these different cell types constitute two functionally specialized subsystems.

The primate visual system is characterized by dozens of distinct cortical areas, each thought to be specialized for the functional analysis of different aspects of the visual environment (1–3). These areas can be divided into a "dorsal" stream specialized for the analysis of spatial relations and a "ventral" stream specialized for object recognition. The functional differences between these areas are believed to arise in part because of differences in contributions from parallel, functionally specialized magnocellular (M) and parvocellular (P) pathways that originate in the retina and terminate in separate layers of primary visual cortex (V1)—layers 4C $\alpha$  and 4C $\beta$ , respectively (2–7). Layer 4C neurons in turn connect to neurons in more superficial layers of V1 that provide the output to "higher"

dorsal and ventral areas. Specifically, ventral stream areas receive inputs directly or indirectly from layer 2/3 of V1, whereas dorsal areas receive their input from layer 4B.

Local circuits in V1 generate two functionally and anatomically distinct channels, "blobs" and "interblobs," contributing to ventral visual areas (2–7). Thus, for the ventral stream, the relationships of M and P pathways to extrastriate areas can be inferred largely from anatomical studies of the connectivity from layer 4C to blobs versus interblobs in layer 2/3 (8–10).

In layer 4B, neurons projecting to different dorsal visual areas or modules (V2 thick stripes, V3, and MT) are spatially intermingled. Thus, anatomical observations of V1 circuitry do not clearly reveal the connective relationships between M and P pathways and the cortical areas that receive layer 4B input (11, 12). Neurons in layer 4B that project to different cortical areas are morphologically distinct. In the macaque monkey, direct input to area MT (V5) comes primarily from spiny stellate neurons (13), whereas areas V2 and V3 also receive input from

pyramidal neurons (14–16). Thus, it is possible to study the different contributions of the M and P pathways to layer 4B-recipient visual areas by using scanning laser photostimulation to identify the sources of functional input to morphologically identified cell types in layer 4B (11, 17–20).

We used scanning laser photostimulation and whole-cell voltage-clamp recordings in living brain slices to identify the locations of neurons providing excitatory input to layer 4B neurons in macaque monkey primary visual cortex (21). Excitatory postsynaptic currents (EPSCs) evoked in the recorded cell after photostimulation are indicative of direct monosynaptic connections from neurons near the stimulation site to the recorded cell. Polysynaptic responses mediated by secondary neurons far from the stimulation site are ruled out because such secondary neurons do not fire action potentials (APs) under the stimulation conditions used (20, 21).

Photostimulation and intracellular recording, along with subsequent anatomical and physiological analyses (22), yielded complete excitatory input maps for 14 layer 4B pyramidal neurons, 4 spiny stellates, and 5 inhibitory neurons. Figure 1 illustrates excitatory input maps to two pyramidal neurons (Fig. 1, A and C), one spiny stellate neuron (Fig. 1B), and one inhibitory neuron (Fig. 1D). All four neurons received strong excitatory input from layer 4C $\alpha$ . Layer 4C $\beta$  provided strong input to the pyramidal neurons but not to the spiny stellate or inhibitory neuron. These characteristics of the excitatory input patterns were typical of the populations for each cell type.

To quantitatively compare input strength across layers for each cell, we calculated the proportion of the excitatory input [estimated evoked input (EEI) (22)] to each cell from each layer by expressing the average value from each layer as a percentage of the sum from all four layers, 4C $\alpha$ , 4C $\beta$ , 5, and 6. These values are shown for all cells in our sample in Table 1. We also calculated the

Systems Neurobiology Laboratories, Salk Institute for Biological Studies, 10010 North Torrey Pines Road, La Jolla, CA 92037, USA.

\*Present address: Department of Neurobiology, Harvard Medical School, 220 Longwood Avenue WAB227, Boston, MA 02115, USA.

†To whom correspondence should be addressed. E-mail: callaway@salk.edu

## REPORTS

statistical significance of measured responses from stimulation sites in each layer by comparing the measured EPSCs after stimulation with spontaneous EPSCs. When the distributions of sums of the peak amplitudes of EPSCs for stimulation trials in a given layer were significantly greater than the same measures from control trials ( $P < 0.05$ , Mann-Whitney U test), the layer was considered to provide significant, detectable input to the cell (see Table 1).

Figure 2A plots the percentage of cells of each type (pyramidal, spiny stellate, and inhibitory) that received significant input from each layer. Every cell except one inhibitory neuron received significant input from layer 4C $\alpha$  (23). Input from other layers was more variable and for layers 4C $\beta$  and 5 depended strongly on cell type. Twelve of 14 pyramidal cells (86%) received significant input from layer 4C $\beta$ , whereas 4C $\beta$  input was detected for none of four spiny stellate neurons (proportions differ significantly;  $P = 0.005$ , Fisher exact test). Significant layer 4C $\beta$  input was

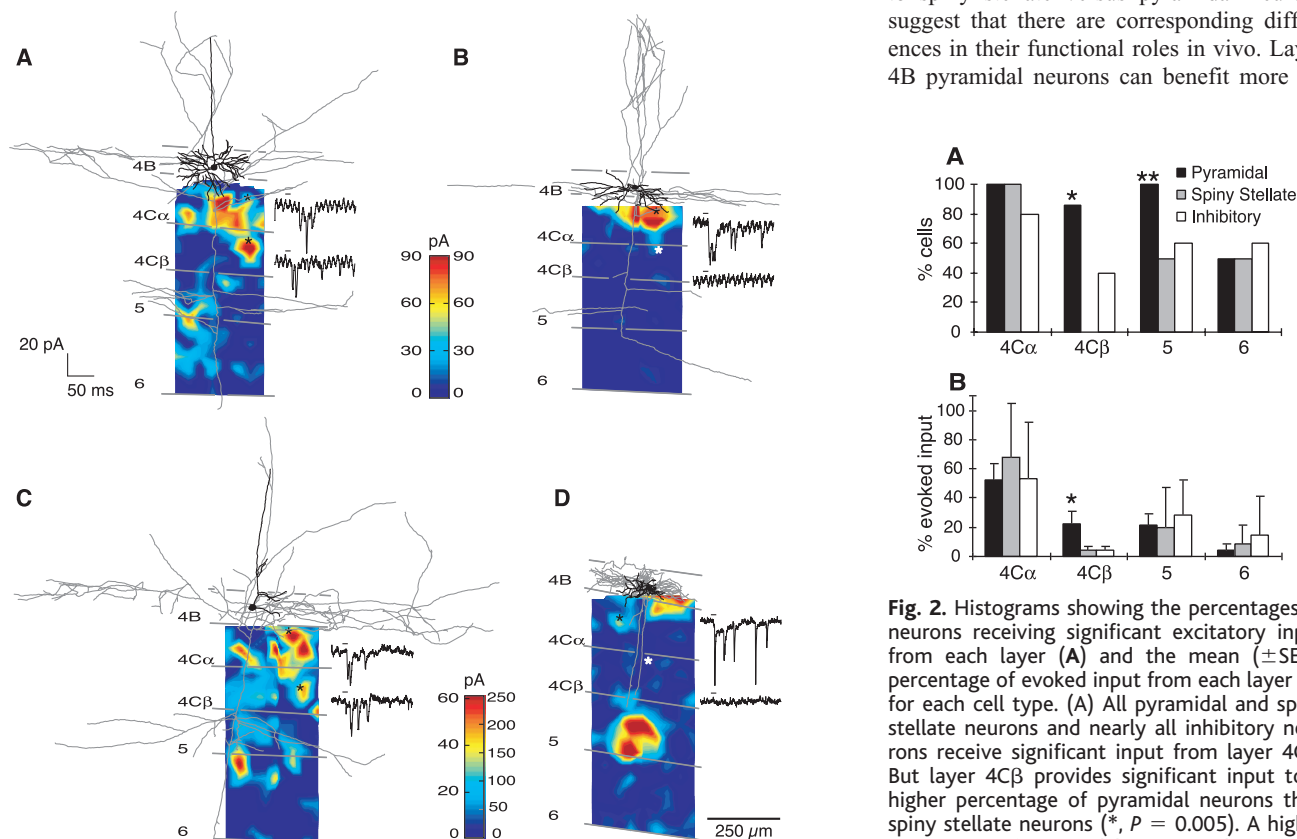
also detected for two of five inhibitory neurons, but this input was much weaker than input to pyramidal neurons (Table 1, see further below). Layer 5 input was also detected more commonly for pyramidal neurons (14 of 14 cells) than for spiny stellate (2 of 4) or inhibitory (3 of 5) cells. About half of the cells received significant input from layer 6, regardless of cell type.

Figure 2B plots the average percentage of EEI from each layer for each cell type. For all cell types, the strongest input was from layer 4C $\alpha$ . For spiny stellate cells, the percentage of EEI from layer 4C $\alpha$  was somewhat greater (68%) than for pyramidal (52%) or inhibitory neurons (53%) (no significant differences). Only pyramidal cells received substantial input from layer 4C $\beta$ . Input from layer 5 was moderate for all cell types, and layer 6 input was relatively weak.

To more directly estimate the relative contributions of the M and P pathways to each cell type, we compared responses after stimulation in the M-recipient layer 4C $\alpha$  with

those after stimulation in the P-recipient layer 4C $\beta$ . For each cell, the mean EEI for layer 4C $\alpha$  was compared with 4C $\beta$ . We calculated a magnocellular dominance index (MDI) (11, 24) by dividing the layer 4C $\alpha$  EEI by the sum of the EEIs for layers 4C $\alpha$  and 4C $\beta$ . Values for MDI ranged from 0.56, or roughly equal input from layers 4C $\alpha$  and 4C $\beta$ , to 1.0—receiving exclusively 4C $\alpha$  input (Table 1). All four spiny stellate neurons in the sample had MDIs greater than 0.9 with a mean of 0.96, indicating 24-fold stronger input from layer 4C $\alpha$  than 4C $\beta$ . Inhibitory neurons were also dominated by layer 4C $\alpha$  input (mean MDI = 0.91). In contrast, pyramidal neurons had significantly lower MDIs (mean MDI = 0.70;  $P < 0.00001$  versus spiny stellate;  $P < 0.001$  versus inhibitory cells) covering a broad range from 0.56 to 0.91 (from balanced to about ninefold stronger 4C $\alpha$  input). The mean value for pyramidal cells corresponds to about twofold stronger input from layer 4C $\alpha$  than from 4C $\beta$ .

The differences in P input from layer 4C $\beta$  to spiny stellate versus pyramidal neurons suggest that there are corresponding differences in their functional roles in vivo. Layer 4B pyramidal neurons can benefit more di-



**Fig. 1.** Laminar excitatory input to layer 4B neurons. Pyramidal neurons receive strong excitatory input from both layers 4C $\alpha$  and 4C $\beta$  (A and C), whereas spiny stellate (B) and inhibitory neurons (D) receive input from layer 4C $\alpha$  but not 4C $\beta$ . Colored maps indicating patterns of excitatory input to each neuron are linear interpolations of the EEI (22) values measured after photostimulation at discrete sites. Colored vertical scale bars indicate the corresponding EEI values for input maps to the left and right. To the right of each input map are example voltage-clamp recordings made while stimulating presynaptic regions (indicated by asterisks) in layer 4C $\alpha$  (top traces) or layer 4C $\beta$  (bottom traces). Short dashes above each recording show the onset of photostimulation. Horizontal lines crossing the input maps represent the anatomical laminar borders. Anatomical reconstructions of dendritic (black) and axonal arbors (gray) are superimposed over the input maps. Scale bars apply to all panels.

**Fig. 2.** Histograms showing the percentages of neurons receiving significant excitatory input from each layer (A) and the mean ( $\pm$ SEM) percentage of evoked input compared with each layer (B) for each cell type. (A) All pyramidal and spiny stellate neurons and nearly all inhibitory neurons receive significant input from layer 4C $\alpha$ . But layer 4C $\beta$  provides significant input to a higher percentage of pyramidal neurons than spiny stellate neurons (\*,  $P = 0.005$ ). A higher percentage of pyramidal neurons also receive significant layer 5 input compared with spiny stellate (\*\*,  $P = 0.04$ ) or inhibitory neurons (not significant). (B) The percentage of evoked excitatory input from layer 4C $\alpha$  is greater than from any other layer for all cell types. Layers 4C $\alpha$ , 5, and 6 each provide similar percentages of the excitatory input to each cell type. But layer 4C $\beta$  provides a significantly higher percentage of the input to pyramidal neurons than to either spiny stellate or inhibitory neurons (\*,  $P < 0.00001$ ).

REPORTS

rectly from information carried in the P pathway than can spiny stellates. But what information is likely to be conveyed? The P pathway is characterized by small, color-opponent receptive fields, whereas the M pathway has larger, achromatic receptive fields (4–7). In these respects, the receptive fields of layer 4B neurons, the majority of which are pyramidal, bear little resemblance to LGN P cells. Layer 4B neurons tend to have large achromatic receptive fields (4–7). The 4B cells differ from both M and P cells, however, in that they are selective for orientation, direction, and binocular disparity (4–7). The P pathway carries information that is potentially useful for the generation of any of these properties. For example, chromatic contrast detected by P cells might contribute to motion detection under low luminance contrast conditions (when M pathway activity is low) (25). Lesion studies suggest an important contribution of the P pathway to stereopsis (7, 26, 27), and cortical areas receiving layer 4B input have large percentages of disparity tuned neurons (4–7). These observations raise the possibility that the P pathway might contribute to disparity tuning of layer 4B pyramids, particularly at high spatial frequencies. Regardless of the functional contributions of the P pathway to layer 4B pyramidal neurons, a more definitive answer could be obtained by directly comparing the visual responses of pyramidal versus spiny stellate neurons or neurons antidromically activated from MT (e.g., 28).

Anatomical considerations indicate that input from layer 4Cβ onto layer 4B pyramidal neurons is likely to be predominantly onto apical dendrites (9, 10). Although the functional significance of this configuration is unknown, we note that the decreased strength of input from layer 4Cβ relative to 4Cα results from a 22% reduction in EPSC amplitude as well as a 38% reduction in EPSC number (29). The differential localization of M versus P input onto pyramidal neuron's dendrites also raises the possibility of selective interactions with other components of the cortical network, such as layer-specific inhibitory connections (30).

The differences in P pathway contributions to layer 4B spiny stellates and pyramids are correlated with differences in the extrastriate areas targeted by each cell type. Area MT receives the majority of its area V1 input from layer 4B spiny stellates (13), whereas area V3 and V2 thick stripes receive mostly pyramidal cell input (14–16). But V3 and V2 thick stripes also supply input to MT, providing an indirect route of influence for the P pathway (2–7). These differences suggest that the quality of the direct input from V1 to MT might be degraded if it were integrated with the P pathway.

The direct versus indirect input paths may be related to the functional heterogeneity of area MT. MT has multiple functional columnar organizations (31–34), and functionally distinct compartments have unique anatomical relationships to higher cortical areas re-

ceiving input from MT (33). These observations suggest that the direct, M pathway-specific input from V1 to MT (through spiny stellates) is likely to target different functional columns than the P-influenced pathways (pyramids) from V2 and V3. Combined functional (2-deoxyglucose) and anterograde anatomical labeling (e.g., 33) from V1, V2, and V3 to MT would allow direct observation of any such relationships. For example, direct spiny stellate input from area V1 may connect preferentially to a particular columnar system that would be degraded by the P pathway, whereas other systems receive P-influenced input from pyramids through V2 or V3.

References and Notes

1. S. M. Zeki, *Nature* **274**, 423 (1978).
2. D. J. Felleman, D. C. Van Essen, *Cerebr. Cortex* **1**, 1 (1991).
3. R. Desimone, L. Ungerleider, in *Handbook of Neuropsychology*, F. Boller, J. Grafman, Eds. (Elsevier, Amsterdam, 1989), vol. 2, pp. 267–299.
4. E. A. DeYoe, D. C. Van Essen, *Trends Neurosci.* **11**, 219 (1988).
5. M. S. Livingstone, D. H. Hubel, *Science* **240**, 740 (1988).
6. S. Zeki, S. Shipp, *Nature* **335**, 311 (1988).
7. W. H. Merigan, J. H. R. Maunsell, *Annu. Rev. Neurosci.* **16**, 369 (1993).
8. E. A. Lachica, P. D. Beck, V. A. Casagrande, *Proc. Natl. Acad. Sci. U.S.A.* **89**, 3566 (1992).
9. E. M. Callaway, *Annu. Rev. Neurosci.* **21**, 47 (1998).
10. N. H. Yabuta, E. M. Callaway, *J. Neurosci.* **18**, 9489 (1998).
11. A. Sawatari, E. M. Callaway, *Nature* **380**, 442 (1996).
12. Anatomical observations of axonal projections from layer 4C reveal that M-recipient neurons in layer 4Cα arborize in layer 4B, whereas P-recipient neurons in layer 4Cβ do not (9, 10). Although a superficial assessment of this observation might suggest that layer 4B neurons cannot receive input from layer 4Cβ, it is important to recognize that layer 4B neurons of all types (spiny stellate, inhibitory, and pyramidal) can extend dendrites into layers 4A and/or 3B, where they overlap with the axons of layer 4Cβ spiny stellates. Furthermore, the axons of layer 4Cβ spiny stellates form synaptic boutons on their unbranched collaterals within layer 4B (10). Indeed, work from this laboratory has previously demonstrated surprisingly robust functional connections from layer 4Cβ onto some layer 4B neurons (17). However, in that study, only five neurons were identified morphologically.
13. S. Shipp, S. Zeki, *Eur. J. Neurosci.* **1**, 309 (1989).
14. A. Burkhalter, D. J. Felleman, W. T. Newsome, D. C. Van Essen, *Vision Res.* **26**, 63 (1986).
15. K. S. Rockland, *Cerebr. Cortex* **2**, 38 (1992).
16. J. B. Levitt, T. Yoshioka, J. S. Lund, *J. Comp. Neurol.* **342**, 551 (1994).
17. E. M. Callaway, L. C. Katz, *Proc. Natl. Acad. Sci. U.S.A.* **90**, 7661 (1993).
18. L. C. Katz, M. B. Dalva, *J. Neurosci. Methods* **54**, 205 (1994).
19. J. L. Dantzker, E. M. Callaway, *Nature Neurosci.* **3**, 701 (2000).
20. A. Sawatari, E. M. Callaway, *Neuron* **25**, 459 (2000).
21. The methods used are identical to those described previously (20). Photostimulation uses ultraviolet (UV) photolysis of "caged glutamate" to locally release the excitatory neurotransmitter glutamate, resulting in depolarization and generation of action potentials in neurons at the release site. Uncaging is spatially restricted because the UV light delivered by an argon-ion laser is focused to a small spot by a ×40 water immersion microscope objective. Control experiments demonstrate that under the stimulation conditions used in these experi-

**Table 1.** Laminar excitatory input for all 23 layer 4B neurons. Each row represents data from a single neuron. The first column identifies each neuron by its morphology as pyramidal, spiny stellate, or inhibitory (types A, B, and C) (23). The next four columns indicate the percentage of the excitatory input (based on EEl) (22) from layers 4Cα, 4Cβ, 5, and 6, respectively, and whether the layer provided statistically significant input (values not in parentheses) or not (values in parentheses). The last column indicates the magnocellular dominance index (MDI, see text) for each cell.

Morphology	4Cα	4Cβ	5	6	MDI
Pyramidal	53.6	19.9	17.9	8.6	0.73
Pyramidal	31.1	23.6	32.6	12.6	0.57
Pyramidal	48.8	19.6	25.6	6.0	0.71
Pyramidal	48.4	16.0	26.4	9.1	0.75
Pyramidal	45.3	32.8	14.4	7.5	0.58
Pyramidal	55.5	26.8	15.4	2.3	0.67
Pyramidal	50.1	30.4	15.9	3.6	0.62
Pyramidal	34.7	27.6	37.1	(0.6)	0.56
Pyramidal	60.9	22.3	16.9	(0.0)	0.73
Pyramidal	48.4	36.6	14.4	(0.6)	0.57
Pyramidal	49.3	19.0	29.5	(2.2)	0.72
Pyramidal	69.4	19.5	10.9	(0.1)	0.78
Pyramidal	65.4	(6.7)	22.3	(5.6)	0.91
Pyramidal	68.2	(7.9)	23.6	(0.4)	0.90
Spiny stellate	67.0	(4.4)	21.4	7.2	0.94
Spiny stellate	15.4	(0.0)	57.6	27.1	1.0
Spiny stellate	93.2	(6.8)	(0.0)	(0.0)	0.93
Spiny Stellate	95.2	(4.8)	(0.0)	(0.1)	0.95
Inhibitory (A)	73.6	(3.2)	(23.2)	(0.0)	0.96
Inhibitory (C)	92.2	(6.2)	(1.7)	(0.0)	0.94
Inhibitory (B)	73.9	6.7	15.4	4.1	0.92
Inhibitory (B)	26.0	5.5	63.9	4.6	0.83
Inhibitory (A)	(0.0)	(0.0)	37.5	62.5	NA

## REPORTS

- ments, photostimulation results in the generation of APs only in neurons with somata close to the stimulation site ( $< \sim 75 \mu\text{m}$ ) (20). Tissue used for preparation of V1 brain slices was collected from the opercular cortical surface of three juvenile *Macaca radiata* under isoflurane anesthesia. The animals were 19, 22, and 23 months old. All procedures that used animals were approved by the Salk Institute Animal Care and Use Committee.
22. For each of the 23 layer 4B neurons in our sample, more than 100 discrete sites (105 to 370, mean = 272) spaced about  $50 \mu\text{m}$  apart and extending vertically in a 250- to  $500 \mu\text{m}$ -wide column across cortical layers 4C $\alpha$ , 4C $\beta$ , 5, and 6 were photostimulated. Later analyses identified individual EPSCs measured after photostimulation (compare Fig. 1). EPSCs measured in recorded cells were distinguished from inward currents evoked directly by uncaged glutamate on the basis of their latency and kinetics (19). The strength of excitatory input from neurons at each stimulation site was estimated by summing together the peak amplitudes of all measured EPSCs and then subtracting the expected contribution from spontaneous EPSCs (measured during no-stimulation control trials) (20). We refer to these values (measured - spontaneous) as estimated evoked input (EEI). To construct input maps (Fig. 1), we spatially smoothed the EEI values at each discrete stimulation site by linear interpolation. Because each site is typically stimulated several times, this display method allows easier visualization of input sources than can be achieved by displaying EEI values at discrete sites. The numbers of stimulation repeats were always the same for sites in each cortical layer. To quantify the relative laminar contributions of excitatory input to each cell, we assigned each stimulation site to the proper cortical layer (19) and then calculated the average EEI for all sites in the layer. In rare cases when average EEI for a layer was negative (spontaneous activity in control trials exceeded measured activity after stimulation), the layer was assigned a value of zero. Because the EEIs are averages per stimulation site, the percentage values for each layer do not account for size differences between layers. Thus, a layer that is relatively large may provide more input than suggested by these values. Each neuron was filled intracellularly with biocytin during recording and its anatomical features reconstructed (10).
  23. Although our sample includes only five inhibitory cells, all appearing to be basket cells with dendrites confined to layer 4B, they fell into three different anatomical classes as defined by Lund and Yoshioka (30). The anatomical differences between cells were observed as differences in the laminar distributions of their axonal arbors. Two cells (Table 1, type A) had extensive axonal arbors in layers 2/3, 4B, and 5 (Lund's type 2). Two cells (Table 1, type B) had axonal arbors primarily in layer 4B (and not above) and secondarily extending to infragranular layers (Lund's type 6). The last cell (Table 1, type C) had a morphology similar to the type A cells, with axonal arbors in layers 2/3 and 4B, but the descending axon collateral also arborized densely in lower layer 4C $\alpha$ , but not deeper. Cells with this morphology were not described by Lund and Yoshioka (30). There were no clear systematic correlations between inhibitory cell type and laminar input sources. Nevertheless, one type A cell had a distinctly different input pattern than any other cell in the population. This type A cell (Table 1, last row) received no significant input from either layer 4C $\alpha$  or 4C $\beta$  but received strong input from layers 5 and 6. This is reminiscent of a subset of inhibitory neurons in layer 2/3 of rat visual cortex that receive dominant input from deep layers (19).
  24. J. H. Maunsell, T. A. Nealey, D. D. DePriest, *J. Neurosci.* **10**, 3323 (1990).
  25. K. R. Dobkins, T. D. Albright, *Vision Res.* **33**, 1019 (1993).
  26. P. H. Schiller, N. K. Logothetis, E. R. Charles, *Nature* **343**, 68 (1990).
  27. ———, *Vis. Neurosci.* **5**, 321 (1990).
  28. J. A. Movshon, W. T. Newsome, *J. Neurosci.* **16**, 7733 (1996).
  29. N. H. Yabuta, A. Sawatari, E. M. Callaway, data not shown.
  30. J. S. Lund, T. Yoshioka, *J. Comp. Neurol.* **311**, 234 (1991).
  31. R. T. Born, R. B. Tootell, *Nature* **357**, 497 (1992).
  32. G. C. DeAngelis, W. T. Newsome, *J. Neurosci.* **19**, 1398 (1999).
  33. V. K. Berezovskii, R. T. Born, *J. Neurosci.* **20**, 1157 (2000).
  34. R. T. Born, *J. Neurophysiol.* **84**, 2658 (2000).
  35. This work was supported by NIH grant EY10742 (E.M.C.). N.H.Y. was supported by NIH training grant EY06837. A.S. was supported by an NIH training grant (GM08107), the Chapman Charitable Trust, the Salk Institute Association, and the Timken-Sturgis Foundation. We thank S. Tye for assistance with animals and J. Dantzer for assistance with data analysis and preparation of figures.

30 November 2000; accepted 15 February 2001

# Tired of waiting for Godot?

## NEW! Science Online's Content Alert Service

Now you can get **instant** summaries of science news and research findings with *Science's* Content Alert Service. This free enhancement to your *Science* Online subscription delivers e-mail summaries of the latest news and research articles published weekly in *Science* - **instantly**. To sign up for the Content Alert service, go to *Science* Online and end the wait.

**Science**  
www.sciencemag.org

For more information about Content Alerts go to [www.sciencemag.org](http://www.sciencemag.org). Click on Subscription button, then click on Content Alert button.